Chemical Science

ROYAL SOCIETY OF CHEMISTRY

EDGE ARTICLE

View Article Online
View Journal | View Issue

Cite this: *Chem. Sci.*, 2025, **16**, 1730

All publication charges for this article have been paid for by the Royal Society of Chemistry

Evolution from $[Zn_9]$ to a record-high $[Zn_{54}]$ subblock and engineering a hierarchical supramolecular framework for enhanced iodine uptake†

Ye Tao,‡[a] Qiubing Dong,‡[c] Jingmeng Wan,[b] Fu-Ping Huang,*[a] Jingui Duan*[bd] and Ming-Hua Zeng*[a]

Hierarchical supramolecular frameworks are being designed and constructed for various applications, yet the controlled assembly and process understanding incorporating giant building blocks remains a great challenge. Here, we report a strategy of "rivet" substitution and "hinge" linkage for the controlled assembly of the hierarchical supramolecular framework. The replacement of two "rivet" ethylene glycol (EG) molecules for triangular prism $[Zn_9]$ (a small block in **1**) with a 1,3-propanediol (PDO) provides space for a "hinge" linkage from adjacent ligands, thus providing a hierarchical (from micro- to mesopores, from the internal cavity to external surface) supramolecular framework (**2**) based on a coordinative subblock with the record number of zinc ions ($[Zn_{54}]$). Time-dependent powder X-ray diffraction and ESI-MS technology were used to assess the *in situ* evolution process: logically progressing from $[Zn_9]$ to $[Zn_{18}]$, then to $[Zn_{27}]$, and finally to $[Zn_{54}]$. The sequential transformation entails two types of half-opening cavities and two types of internal microcages. Further aggregation of $[Zn_{54}]$ in dia topology engenders the formation of a one-dimensional channel (10 Å), and an additional mesocage with a volume of 16 × 16 × 55 $Å^3$. The diverse pore system exhibits an impressive uptake capability (3.19 g g^{-1}) for iodine vapor at 75 °C and effective ethylene purification. Our investigations represent a valuable avenue for assembling a giant subblock and hierarchical supramolecular framework, facilitating multi-functional molecular accommodation.

Received 6th July 2024
Accepted 6th December 2024

DOI: 10.1039/d4sc04474f

rsc.li/chemical-science

Introduction

The interest in supramolecular chemistry has progressively increased with the synthesis of intricate structures.[1–5] This is because the use of "programmed" building blocks allows for the assembly of cluster- or spacer-based supramolecules with unique physicochemical properties compared to their precursors.[6–9] Interestingly, spacer-based supramolecules (*e.g.* coordination cages) exhibit promising cavities, which show emerging functions, such as synergistic catalysis, ionic conductivity, enantioselective recognition, and gas separation.[10–12]

Analogous to metal–organic frameworks,[13] coordination-driven assemblies, together with non-interfering interactions, have emerged as an effective approach for the construction of spacer-based supramolecules.[14–19] For example, the coordination between palladium(II) and the ligand (with a bending angle of 149°) selectively assembles into a $[Pd_{24}L_{148}]$ complex.[20] However, when the bending angle of the ligand is increased to 152°, a supramolecule of $[Pd_{30}L_{260}]$ can be assembled, with 144 components and a type of nearly spherical cage (~6.8 nm).[21] Similarly, a cuboctahedral nanocage, containing 13 cavities, but two types only, has been prepared from a C_{3v}-symmetric ligand, where the pregnant molecular nanoball can be converted into a single nanoball by ligand (C_{2v}) exchange.[22] Therefore, the changes in geometric complementarity, the steric constraints, and also the external stimuli can influence the self-assembly of the subunits. In other words, the preparation of desired

[a]*State Key Laboratory for Chemistry and Molecular Engineering of Medicinal Resources, School of Chemistry & Pharmaceutical Sciences, Guangxi Normal University, Guilin 541004, China. E-mail: huangfp2010@163.com; zmh@mailbox.gxnu.edu.cn*

[b]*State Key Laboratory of Materials-Oriented Chemical Engineering, College of Chemical Engineering, Nanjing Tech University, Nanjing 211816, China. E-mail: duanjingui@njtech.edu.cn*

[c]*College of Chemistry and Materials Science, Anhui Normal University, Wuhu, Anhui 241000, China*

[d]*State Key Laboratory of Chemistry and Utilization of Carbon-Based Energy Resources, College of Chemistry, Xinjiang University, Urumqi, 830017, China*

† Electronic supplementary information (ESI) available: Synthesis of these two crystals, ESI-MS, SEM, PXRD, TGA, UV, IR, sorption isotherms, IAST, and breakthrough experiments. CCDC 2323878–2323880. For ESI and crystallographic data in CIF or other electronic format see DOI: https://doi.org/10.1039/d4sc04474f

‡ These authors contributed equally to this work.

architectures by molecular self-assembly with a few or dozens of components, as well as the accurate understanding and regulation of the interplays involved, is still inherently challenging, and particularly huge when it comes to the one with a hierarchical (from micro- to mesopores and from the internal cavity to external surface) pore system established from a large number of components (>100) comparable to that seen in nature, and has been rarely reported.[21,23]

During our exploration of coordinative clusters,[24–29] a series of M_4 cubane and M_7 brucite disk clusters, a cubane-based triangular [Co_{12}] single-molecule magnet, and the largest chiral cobalt cluster of [Co_{16}] have been synthesized.[27] According to the structural correlation information of the solid/solution phase using mass spectrometry technology, the transformation mechanisms of step-by-step assembly, competitive assembly, assembly/disassembly/*in situ* reaction/reassembly were proposed. This crucial and fundamental information not only helps to gain insights into the evolution of molecular fragments but also contributes to developing effective strategies for controllable assembly. Given the observation on the assembly process of the [Co_{16}] supercluster, a new structure with separate Co_4O_4 cubes has been prepared after step-by-step elimination and substitution of inner bridging ligands. However, the tuned assembly makes both the size and components of the sub-block smaller, restricted by the flexible configuration and the limited coordination sites.

To reverse this trend and also to enrich the family of supramolecular chemistry, we report here a strategy of "rivet" substitution and "hinge" linkage for the controlled assembly of a hierarchical supramolecular framework with a giant subunit from that with a small cluster (Scheme 1). To achieve this goal, a judicious choice of appropriate molecular building blocks is very important. The ligand (6,6′-(1*H*,1*H*′-[3,3′-bi(1,2,4-triazole)]-5,5′-diyl)dipicolinic acid: H_4btdpa) was selected for the following reasons: (a) three types of coordination groups of carboxylate, pyridine, and triazole were integrated into one linear-dentate shape ligand with twelve sites to bind metal ions, (b) the inner pyridine-triazole skeleton supports bidirectional coordination capacity while the two terminal carboxylate groups provide significant potential to extend the superstructure, (c) the multiple ring rotation around the C–C bond between adjacent structural motifs (four aromatic rings and two carboxylates) facilitates linker flexibility for self-adjusted coordination; (d) the large dimensions of the ligand may meet the demand for stabilizing nanoclusters/nanocages.[32] Additionally, of the 3d metal ions, zinc is particularly attractive in terms of its relative flexibility in adopting different coordination environments, including the coordination number and geometry. Based on these considerations, a supramolecule **1** was prepared at first, in which the ethylene glycol (EG) strengthens the small triangular prism [Zn_9] subcluster. After replacing these short "rivet" molecules with relatively longer 1,3-propanediol (PDO), extra coordination sites on terminal Zn ions on [Zn_9] were linked together through the "hinge" carboxylates in btdpa, forming a giant [Zn_{54}] nanocage (114 components) with four kinds of micropores. Further aggregation of this nanocage in dia topology offers a new superstructure with significant mesopores (55 Å), allowing impressive capabilities in iodine adsorption and ethylene purification.

Results and discussion

Rhombic crystals of **1** ([Zn_9(btdpa)$_3$(EG)$_6$]·5.5H_2O) were obtained through the solvothermal reaction of H_4btdpa, $Zn(NO_3)_2$·6H_2O and EG. **1** crystallizes in the $R\bar{3}c$ space group (Tables S1 and S2†). In **1**, three linearly packed Zn ions are connected by two ligands at an angle of about 60°, forming a triangular prism nanotube. Additionally, each edge of this

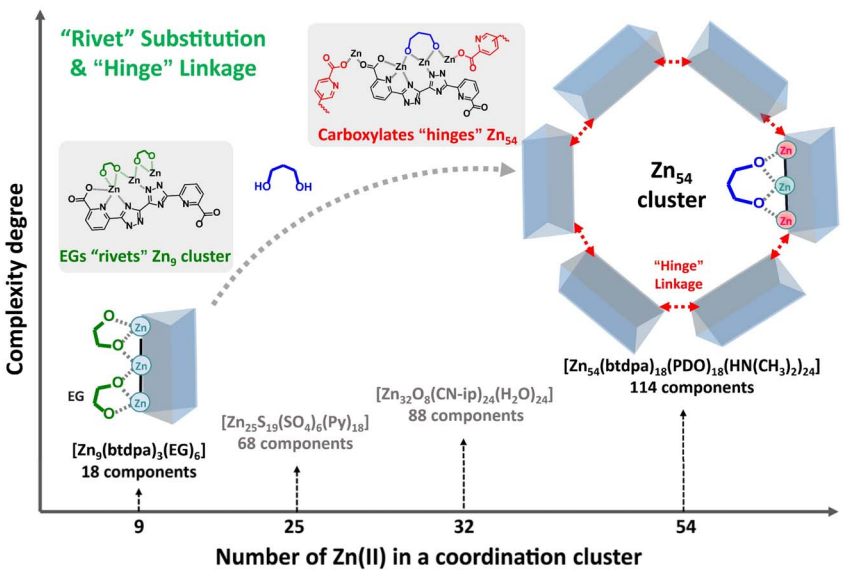

Scheme 1 Illustration of the strategy of "rivet" substitution and "hinge" linkage for controlled assembly of a giant coordinative cluster ([Zn_{54}]) from a small one ([Zn_9]) in the supramolecular framework, in comparison with previous benchmark Zn(II) clusters.[30,31]

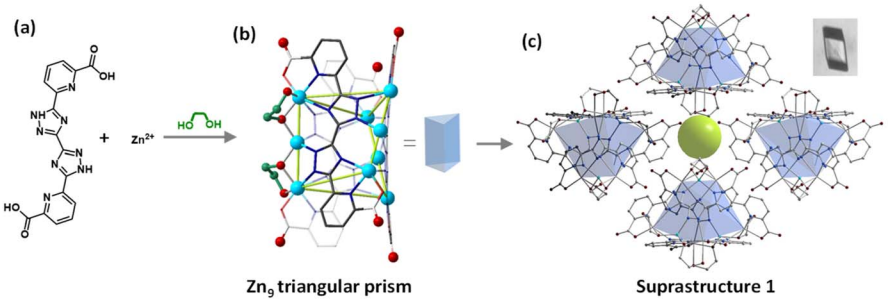

Fig. 1 Schematic representation of the synthesis and structure of supramolecule **1**: involving a ligand and metal center (a), structure view of **1** (b) and its packing mode (c), inset c is the photo of **1**. H atoms were omitted for clarity.

cluster is strengthened by two "rivet" EGs (Fig. 1a and b), where the two O atoms adopt the μ_2-η^1,η^2 mode. The nanotubes are connected by hydrogen bonds (O_{COO}–H–O_{EG}) and form a supramolecular framework with small channels of about 4.4 Å (Fig. 1c and S2†). In this regard, if the two "rivet" molecules on the edge of **1** can be replaced by a molecule with two O atoms in the μ_3-η^2,η^2 mode, there may be extra space on the two terminal Zn atoms, allowing for coordination expansion as subunits.

To ensure the μ_3-η^2,η^2 mode, the distance between the two O atoms on the "rivet" should fit the configuration of the trinuclear edges in **1**. Compared with EG, PDO with three carbons in the center may be a candidate. To validate this idea, **1** was soaked in a PDO/*N*,*N*′-dimethylformamide (DMF) solution for the synthesis of the supramolecule with an expanded subunit. As expected, octahedral crystals $[Zn_{54}(btdpa)_{18}(PDO)_{18}(HN(CH_3)_2)_{21.6}]\cdot 16PDO\cdot 30DMF$ (**2**) were found (Fig. 2), which has a coordinative cluster with the largest number of Zn(II) ions, compared to the benchmark clusters with 25 and 32 Zn(II) ions (Fig. S3†).[30,31] The crystal has a cell volume of up to 198 173 Å^3 in the $Fd\bar{3}$ space group. Firstly, it is found that the regular triangular prism of **1** changed to become a highly distorted one, because two of the three [Zn–Zn–Zn] edges were not straight anymore. The two μ_2-η^1,η^2 EGs on each edge of **1** have been replaced by one μ_3-η^2,η^2 PDO, that is, there are just three PDO molecules for each Zn_9 species in **2** (Fig. S1–S4†). There is an obvious coordination number lowering from single μ_6-fashion through ten coordination atoms in **1** to mixed μ_5-coordination through nine atoms and μ_4-coordination through eight atoms in **2** for the primary ligand of btdpa.

Even so, the pyridine–triazole part in each independent btdpa still adopts the bilateral coordination with four Zn(II) moieties. Coupled with μ^3-chelated PDO linkage of another

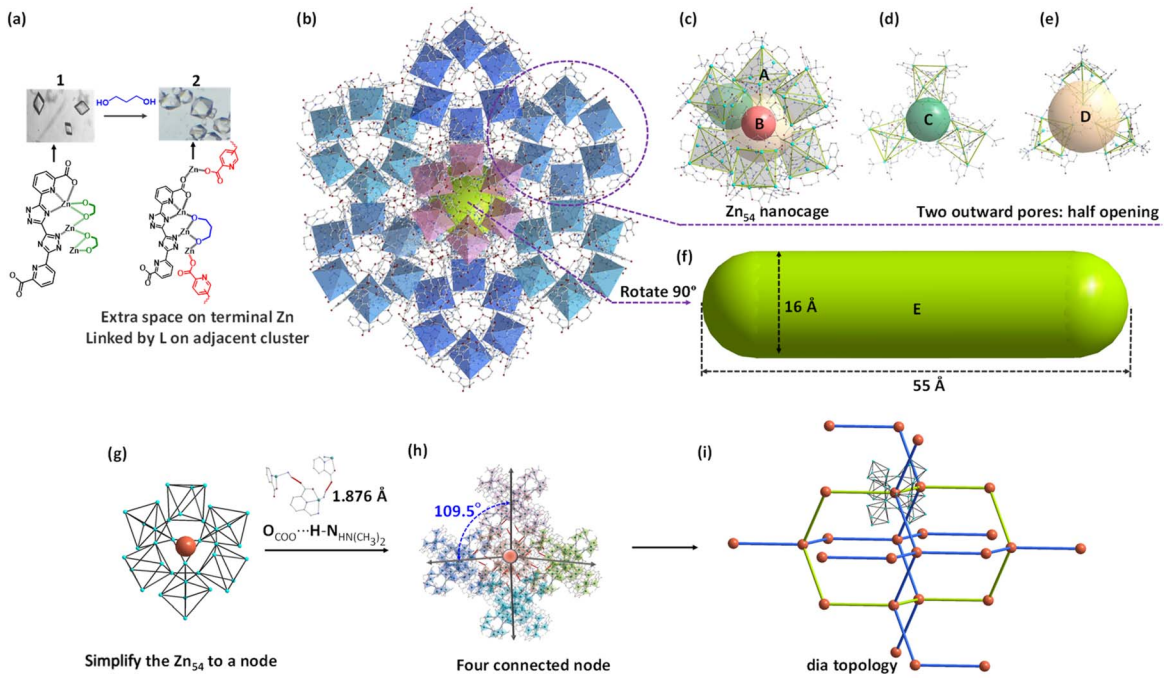

Fig. 2 Schematic representation of the synthesis, structure, and topology of **2**: synthesis route and associated coordination change of the blocks before and after reaction (a); packing view of structure **2** (b), view of **2** and its four kinds of micropores (c–e); view of the mesopore generated by aggregation of [Zn_{54}] (f); simplified geometry of Zn_{54} (g) and the hydrogen-bond connected network (h); dia topology (i), the green line indicates the macropore again.

Zn(II), the nano-nuclear building block can be maintained. The coordination changes in the inner pyridine-triazole strut also promote the slacking of the whole btdpa ligand, confirmed by the five independent Zn(II) moieties with a more regular polyhedron geometry, and larger/multiple ring rotation of btdpa in **2**, compared to that of **1** (Tables S3–S5†). As the concomitant benefit, one of the terminal carboxylates previously adopted μ_1-η^1 fashion transform to the μ_2-η^1,η^1 model using both of the two oxygen atoms, leading to the desired role of the carboxylate "hinge" to link two adjacent Zn_9-subunits. As a result, a giant nanocage of [Zn_{54}] with an octahedron configuration was constructed from six Zn_9-subunit blocks. The diameter of this cluster reaches 35.6 Å, comparable in size to some biological molecules (Fig. S5†). Thanks to the involved hydrogen bonds, the [Zn_{54}] aggregates together to form a supramolecular framework (Fig. 2b).

The structure of [Zn_{54}] is fascinating. The triangular prism nanotube in **1** distorts into an octahedral Zn_9-subunit (pore A) with an internal size of about 4.2 Å in **2** (Fig. S6†). In contrast to the usual pore expansion due to increased components, the coordination extension of the Zn_9-subunit in **2** leads to a collapsible arrangement with a central pore B measuring only 5.8 Å (Fig. 2c and S7†). This collapsible arrangement offers two types of bowl-shaped pores (C and D). The lower part of pore C is composed of three PDO molecules, while the upper part is made up of three Zn_9-subunits, resulting in an opening size of 11.0 Å and a depth of 12.6 Å (Fig. 2d and S8†). Next to pore C is another bowl-shaped pore D, which is wider (13.2 Å) but shallower (8.3 Å) (Fig. 2e and S9†). Additionally, six hydrogen bonds of $O_{COO}\cdots H\text{–}N_{HN(CH_3)_2}$ with a short distance of 1.876 Å have been found between the two adjacent [Zn_{54}] clusters, yielding additional mesopore *E* ($\sim 16 \times 55$ Å^2) and a 1D channel (10 Å) along the [1 1 0] plane (Fig. 2f and S10†). Supramolecular chemistry has yielded fruitful results, whereas the creation of six different types of nanospaces, particularly ranging from micro-to mesopores, is unprecedented. To better understand structure **2**, topology analysis was performed. Considering the four groups of hydrogen-bonds around [Zn_{54}], this subunit can be simplified as a 4-fold-connected node. After subsuming these doubly connected vertices into the linkage, a net with a **dia** topology was observed (Fig. 2g–i). Notably, the solvent-accessible volume calculated for the framework of **2** using PLATON is *ca.* 58.3%, which is almost five times larger than that of **1** (12.9%). The structures and phase purities of the as-synthesized **1** and **2** were confirmed by powder X-ray diffraction (PXRD) analyses (Fig. S11–S14†).

Based on these structures, it is evident that the strategy of "rivet" substitution and "hinge" linkage is effective for the controlled assembly of a supramolecular framework with a giant subunit from a much smaller one. Therefore, delving into the molecular-level replacement of the "rivet" may offer valuable insights into this strategy. During the reaction of **1** to **2**, the uniformly dispersed crystals were evaluated by PXRD, while the corresponding solvent was detected by electrospray ionization mass spectrometry (ESI-MS).

As shown in Fig. 3a, the position of the typical [1 0 −2] peak of **1** did not change obviously after 2 hours of reaction, but became slightly broader and was associated with a very small shoulder peak. As the reaction progressed, the intensity of this shoulder peak gradually increased, causing the [1 0 −2] peak to split into two at 4 hours of reaction. This change indicates that 1 does not dissolve in the solvent and maintains its crystallinity initially. After 8 hours, the four peaks ([4 0 0], [3 3 1], [4 2 2], and [5 1 1]) belonging to 2 were observed, while the [1 0 −2] peak belonging to 1 disappeared. This indicates a gradual extension of the substitution reactions from the outside to the inside of the bulky crystal 1. This is because the presence of macrospores in 2 allows for convenient molecular exchange. Moreover, the relative intensity of the diffraction peaks of the collected crystals at 12 hours became much stronger than that at 8 hours, showing a completed "rivet" substitution and "hinge" linkage. This result has also been confirmed by time-dependent IR and Raman spectroscopy (Fig. S16 and S17†). In addition, the non-observable signal in the range of $m/z = 1400$ to 4000 of the reaction solvents confirms that the "rivet" substitution and "hinge" linkage occurs initially on the crystal surface and then extends into the crystal as the reaction progresses (Fig. S18†).

Due to the *in vivo* reaction, the gradual change process cannot be monitored at the molecular level by solvent ESI-MS. However, the dissociation of **2** provides valuable insight into the structural transformation (Fig. 3b and c, S19–S20†). The main species were found at 0 eV. These can be identified as the ion fragments of Zn_9^-, Zn_{18}^- and Zn_{27}^{2-} by comparing the simulated and experimental isotope distributions. When the voltage was increased to 20 eV, the abundance of the Zn_{27}^{2-} ion peak decreased. This indicates further fragmentation of the Zn_{27}^{2-} species into smaller fragments. Therefore, the assembly of the [Zn_{54}] nanocluster may occur through the following process: EG is replaced by PDO on a [Zn_9] cluster, the carboxylate O of a ligand from another Zn_9 joins the coordination of the terminal Zn atoms, forming Zn_{18} and then Zn_{27} units. Further coordination from carboxylate O fuses two Zn_{27} units together to form a [Zn_{54}] nanocluster (Fig. 3d).

The permanent porosities of **1** and **2** were evaluated using N_2 (77 K) adsorption isotherms (Fig. 4a and b). The rapid gas uptake at a lower pressure area can be attributed to the adsorption in micropores, while the uptake at the pressure of $P/P_0 = 0.1$–0.2 can be assigned as the adsorption in micro- and mesopores. In contrast, **1** exhibits negligible adsorption of N_2. The Brunauer–Emmett–Teller surface area of **2** was calculated to be 736 m^2 g^{-1}. Additionally, the evaluated pore size distribution varies in a wide range of ~6 to 55 Å (Fig. 4b), agreeing well with the crystal structure.

The intriguing pore system encourages us to explore the function of **2**. Given that radioactive I^{129} with an extremely long half-life of up to 15.7 million years is a heavy waste in nuclear power stations, a new type of adsorbent with strong I_2 affinity and high uptake is quite useful for clean nuclear energy production. After exposure of activated **2** to iodine vapor at 75 °C, the maximum iodine absorption capacity reaches 3.19 g g^{-1} (Fig. 4c). To the best of our knowledge, such iodine uptake data not only represents a new record in the metal–organic cage (previous record of 2.35 g per g AlOC-162-C)[33] or cluster-based adsorbents (2.246 g g^{-1} for $Ti_{12}Pb_5$ based porous layers),[34] but

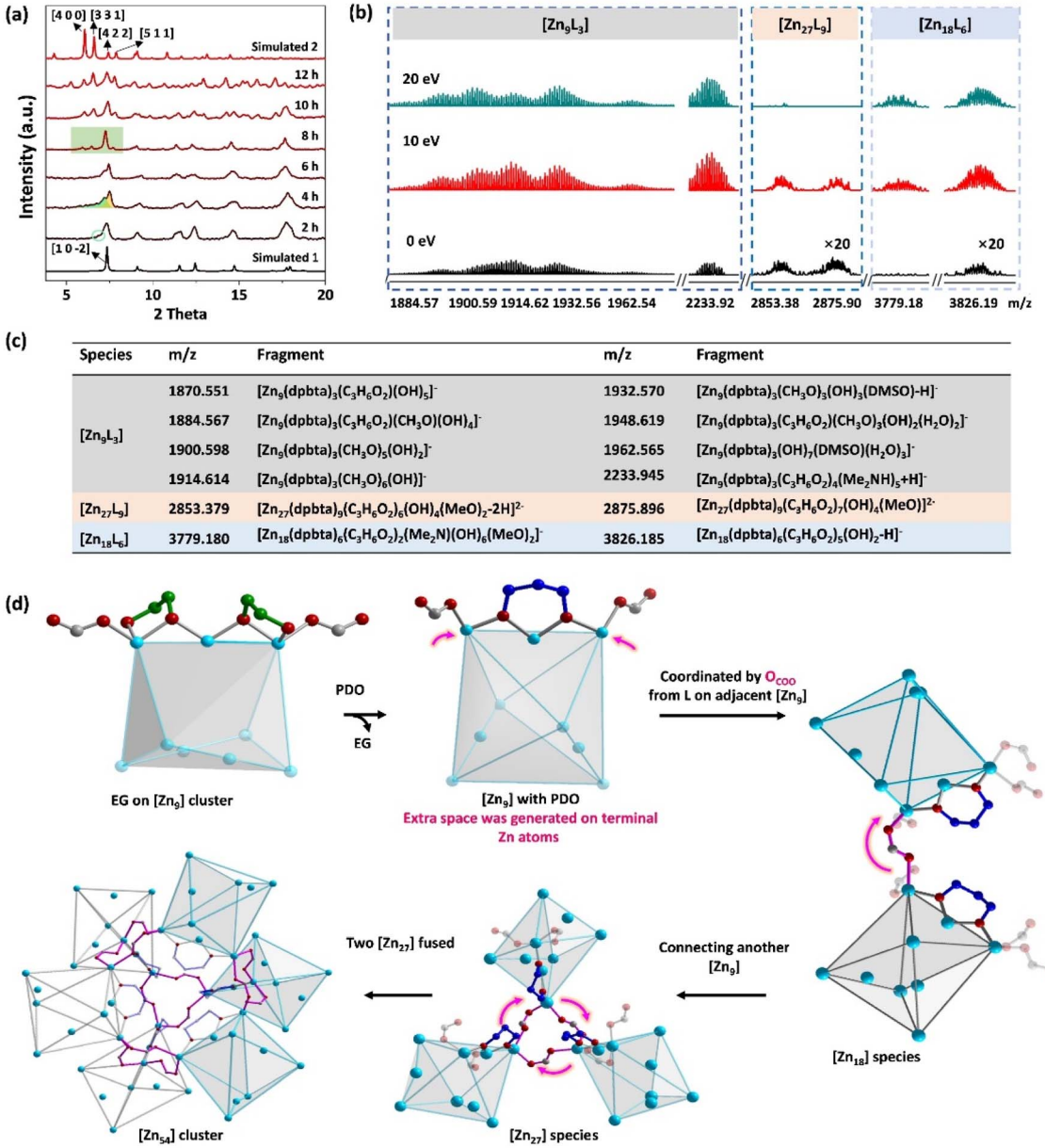

Species	m/z	Fragment	m/z	Fragment
$[Zn_9L_3]$	1870.551	$[Zn_9(dpbta)_3(C_3H_6O_2)(OH)_5]^-$	1932.570	$[Zn_9(dpbta)_3(CH_3O)_3(OH)_3(DMSO)\text{-}H]^-$
	1884.567	$[Zn_9(dpbta)_3(C_3H_6O_2)(CH_3O)(OH)_4]^-$	1948.619	$[Zn_9(dpbta)_3(C_3H_6O_2)(CH_3O)_3(OH)_2(H_2O)_2]^-$
	1900.598	$[Zn_9(dpbta)_3(CH_3O)_5(OH)_2]^-$	1962.565	$[Zn_9(dpbta)_3(OH)_7(DMSO)(H_2O)_3]^-$
	1914.614	$[Zn_9(dpbta)_3(CH_3O)_6(OH)]^-$	2233.945	$[Zn_9(dpbta)_3(C_3H_6O_2)_4(Me_2NH)_5\text{+}H]^-$
$[Zn_{27}L_9]$	2853.379	$[Zn_{27}(dpbta)_9(C_3H_6O_2)_6(OH)_4(MeO)_2\text{-}2H]^{2-}$	2875.896	$[Zn_{27}(dpbta)_9(C_3H_6O_2)_7(OH)_4(MeO)]^{2-}$
$[Zn_{18}L_6]$	3779.180	$[Zn_{18}(dpbta)_6(C_3H_6O_2)_2(Me_2N)(OH)_6(MeO)_2]^-$	3826.185	$[Zn_{18}(dpbta)_6(C_3H_6O_2)_5(OH)_2\text{-}H]^-$

Fig. 3 PXRD patterns of the time-dependent reaction from **1** to **2** (a), ESI-MS of dissociated **2** and typical peaks (b and c), and predicted conversion process from **1** to **2** (d).

also approaches those of best-performing pure MOFs like MOF-808 (2.18 g g^{-1}),[35] $[Zr_6O_4(OH)_4(L^7)_6]$ (2.79 g g^{-1}),[36] UPC-158-HCl (2.92 g g^{-1}),[37] and PCN-333-Al (4.42 g g^{-1})[38] (Table S6†).[39] In addition, iodine enrichment can also be performed in solution.[40] It is notable that the iodine-loaded single crystal structure disclosed that the disordered iodine species are mainly concentrated in pore C, which might be ascribed to the abundance of triazole and pyridine nitrogen atoms on the surface of this pore (Fig. S21†). Meanwhile, these adsorbed iodine species can be released by immersing the I_2@**2** in ethanol at room temperature (Fig. S22†).

To extend the functionality of **2**, single-component adsorption isotherms of C_2H_2, CO_2, and C_2H_4 were collected. **2** shows a relatively higher C_2H_2 uptake (40.6 cm^3 g^{-1}) compared to CO_2 (24.2 cm^3 g^{-1}) and C_2H_4 (17.8 cm^3 g^{-1}) at 298 K and 1 bar, showing potential for C_2H_4 purification (Fig. S23–S33†). To confirm this, dynamic breakthrough experiments were performed with the binary mixtures (C_2H_2/C_2H_4, 1/99, v/v, 2 mL min^{-1}) on **2**. Pure C_2H_4 (6.6 min) eluted first from the column, while C_2H_2 broke through the sample at 18.6 min (Fig. S34†). The pure C_2H_2 (>99.5%) was also obtained *via* the subsequent desorption process. After changing the feed gas to a ternary mixture of $C_2H_2/CO_2/C_2H_4$ (1/9/90, v/v/v), C_2H_4 and CO_2 were eluted at 9.8 min and 15.7 min, respectively, while C_2H_2 broke through at 23.3 min (Fig. S35†). The obvious intervals confirmed that **2** retains the ability to purify C_2H_4 from mixtures containing C_2H_2 or CO_2/C_2H_2, confirmed by the calculated selectivity and binding energy (S28–S33†). Furthermore, no loss

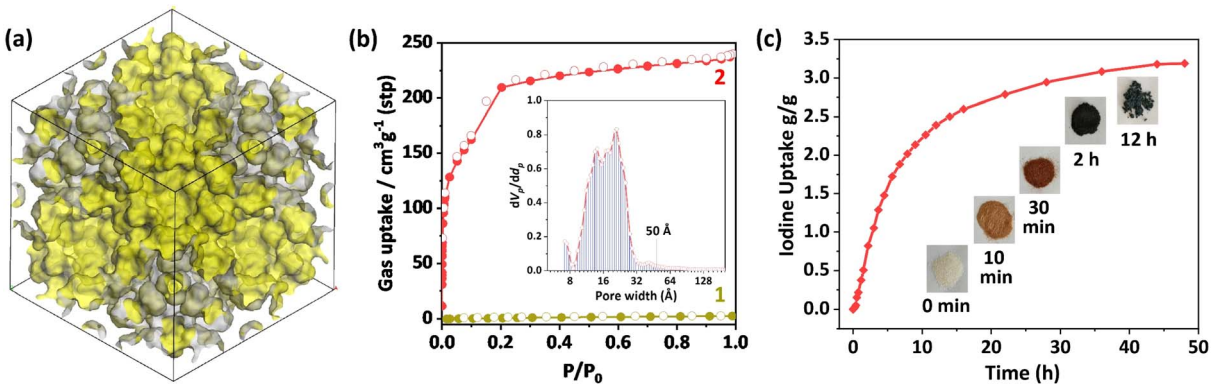

Fig. 4 (a) Accessible inner surface highlighted as yellow in a unit cell of **2**. (b) The 77 K N_2 adsorption isotherms of **1** and **2**, and the measured pore size distribution of **2**. (c) The time-dependent iodine vapor uptake performance of **2** at 75 °C under ambient pressure.

of capacity was observed during the cycling experiments, confirming the good framework stability of this hierarchical supramolecular framework (Fig. S36†).

Conclusions

We report a strategy of "rivet" substitution and "hinge" linkage for the controlled assembly of a hierarchical supramolecular framework. The rational design of a particular primary ligand, in combination with the auxiliary ligand and the Zn(II), provides a mother supramolecular **1** with a small Zn_9 sub-cluster. The replacement of the "rivet" auxiliary ligands on Zn_9 by a flexible and longer one provides space for "hinge" linkage from adjacent ligands, yielding a complex and giant cluster ([Zn_{54}] with 114 components) that has the largest number of Zn(II) ions and four types of micropores. Aggregation of the [Zn_{54}] cluster in **dia** topology creates a hierarchical supramolecular mesostructured **2** (~55 Å), facilitating a record iodine vapor uptake (3.19 g g^{-1}) among cage or cluster type sorbents, as well as effective C_2H_2/C_2H_4 and C_2H_2/CO_2 separation. More importantly, the *in situ* substitution and linkage processes have been finely revealed *via* spectra and diffraction analysis. Such synergistic incorporation not only facilitates the construction of an unprecedented structure but also illustrates the importance of multidentate and self-adjusting ligands in oriented assembly that can have profound implications in coordination-driven supramolecular chemistry. Moving forward, the molecular insights of this strategy can be extended as an innovative tool for the advancement and enrichment of supramolecular families.

Data availability

All data can be found in the main text and ESI.†

Author contributions

M.-H. Z., J. D., and F.-P. H. conceived the idea of this work. Y. T., Q. D., and J. W. carried out the experiments and analysed the results. J. D., Q. D. and M.-H. Z. wrote the paper. All authors participated in discussions and gave valuable suggestions for the final draft.

Conflicts of interest

The authors declare no conflict of interest.

Note added after first publication

This version replaces the manuscript published on 11th December 2024 which contained a typographical error in the title. The RSC apologises for any confusion.

Acknowledgements

This work was supported by the BAGUI talent program in Guangxi Province (No. 2019AC26001), the National Natural Science Foundation of China (U23A2080, 22171075, 22401005, 22171135, 22471235, 22075056, and 21861005), the National Natural Science Foundation of Jiangsu Province (BK20231269) and the Peak Discipline Construction Project (No. 1023005).

References

1 A. V. Virovets, E. Peresypkina and M. Scheer, *Chem. Rev.*, 2021, **121**, 14485–14554.
2 R. Jin, C. Zeng, M. Zhou and Y. Chen, *Chem. Rev.*, 2016, **116**, 10346–10413.
3 R. J. Severinsen, G. J. Rowlands, P. G. Plieger and J. I. Pheno, *Macromol. Chem.*, 2019, **96**, 29–42.
4 F. Yu, M. Kurmoo, G.-L. Zhuang and J.-L. Zuo, *Chem. Sci.*, 2018, **9**, 7498–7504.
5 D. l. Caulder and K. N. Raymond, *Acc. Chem. Res.*, 1999, **32**, 975–982.
6 L.-L. Yan, L.-Y. Yao, M. Ng and V. W.-W. Yam, *J. Am. Chem. Soc.*, 2021, **143**, 19008–19017.
7 F. J. Rizzuto, L. K. S. von Krbek and J. R. Nitschke, *Nat. Rev. Chem*, 2019, **3**, 204–222.
8 G. W. V. C. R. M. McKinlay and J. L. Atwood, *Proc. Natl. Acad. Sci. U. S. A.*, 2005, **102**, 5944–5948.

9 T. R. Cook, Y.-R. Zheng and P. J. Stang, *Chem. Rev.*, 2012, **113**, 734–777.
10 X.-Y. Zheng, Y.-H. Jiang, G.-L. Zhuang, D.-P. Liu, H.-G. Liao, X.-J. Kong, L.-S. Long and L.-S. Zheng, *J. Am. Chem. Soc.*, 2017, **139**, 18178–18181.
11 G. L. Zhang, L. P. Zhou, D. Q. Yuan and Q. F. Sun, *Angew. Chem., Int. Ed.*, 2015, **54**, 9844–9848.
12 A. J. Tasiopoulos, A. Vinslava, W. Wernsdorfer, K. A. Abboud and G. Christou, *Angew. Chem., Int. Ed.*, 2004, **43**, 2117–2121.
13 H.-C. Zhou, J. R. Long and O. M. Yaghi, *Chem. Rev.*, 2012, **112**, 673–674.
14 L.-L. Yan and V. W.-W. Yam, *J. Am. Chem. Soc.*, 2023, **146**, 609–616.
15 H.-K. Liu, T. K. Ronson, K. Wu, D. Luo and J. R. Nitschke, *J. Am. Chem. Soc.*, 2023, **145**, 15990–15996.
16 X.-R. Liu, P.-F. Cui, S.-T. Guo, Y.-J. Lin and G.-X. Jin, *J. Am. Chem. Soc.*, 2023, **145**, 8569–8575.
17 K. Wang, J. H. Jordan, X. Y. Hu and L. Wang, *Angew. Chem., Int. Ed.*, 2020, **59**, 13712–13721.
18 A. Dhamija, C. K. Das, Y. H. Ko, Y. Kim, R. D. Mukhopadhyay, A. Gunnam, X. Yu, I.-C. Hwang, L. V. Schäfer and K. Kim, *Chem*, 2022, **8**, 543–556.
19 H. Takezawa, K. Shitozawa and M. Fujita, *Nat. Chem.*, 2020, **12**, 574–578.
20 J. Bunzen, J. Iwasa, P. Bonakdarzadeh, E. Numata, K. Rissanen, S. Sato and M. Fujita, *Angew. Chem., Int. Ed.*, 2012, **51**, 3161–3163.
21 D. Fujita, Y. Ueda, S. Sato, N. Mizuno, T. Kumasaka and M. Fujita, *Nature*, 2016, **540**, 563–566.
22 I. A. Bhat, D. Samanta and P. S. Mukherjee, *J. Am. Chem. Soc.*, 2015, **137**, 9497–9502.
23 Q.-F. Sun, J. Iwasa, D. Ogawa, S. S. Yoshitaka Ishido, T. Ozeki, Y. Sei, K. Yamaguchi and M. Fujita, *Science*, 2010, **328**, 1144–1147.
24 Y. F. Wang, Y. Liang, Y. F. Wu, J. Yang, X. Zhang, D. Cai, X. Peng, M. Kurmoo and M. H. Zeng, *Angew. Chem., Int. Ed.*, 2020, **59**, 13232–13237.
25 Y. Huang, J. Wan, T. Pan, K. Ge, Y. Guo, J. Duan, J. Bai, W. Jin and S. Kitagawa, *J. Am. Chem. Soc.*, 2023, **145**, 24425–24432.
26 Z. Lu, L. Du, R. Guo, G. Zhang, J. Duan, J. Zhang, L. Han, J. Bai and J. T. Hupp, *J. Am. Chem. Soc.*, 2021, **143**, 17942–17946.
27 Y.-Q. Hu, M.-H. Zeng, K. Zhang, S. Hu, F.-F. Zhou and M. Kurmoo, *J. Am. Chem. Soc.*, 2013, **135**, 7901–7908.
28 Y.-L. Zhou, M.-H. Zeng, L.-Q. Wei, B.-W. Li and M. Kurmoo, *Chem. Mater.*, 2010, **22**, 4295–4303.
29 J. Wang, Y. Jiang, J. Y. Liu, H. B. Xu, Y. X. Zhang, X. Peng, M. Kurmoo, S. W. Ng and M. H. Zeng, *Angew. Chem., Int. Ed.*, 2021, **60**, 22368–22375.
30 J. M. Seco, I. Oyarzabal, S. Pérez-Yáñez, J. Cepeda and A. Rodríguez-Diéguez, *Inorg. Chem.*, 2016, **55**, 11230–11248.
31 C. Xue, J. Zhang, X. Wang, M. Gu, Y. Zhu, D.-S. Li, J. Guo, Y. Liu and T. Wu, *Chem. Commun.*, 2019, **55**, 8146–8149.
32 P. Alborés and E. Rentschler, *Angew. Chem., Int. Ed.*, 2009, **48**, 9366–9370.
33 N. Yang, S. T. Wang, C. S. Li, J. Zhang, M. Y. Zhang and W. H. Fang, *Small*, 2024, 2311083.
34 A. Said, C. Gao, C. Liu, H. Niu, D. Wang, Y. Liu, L. Du, C.-H. Tung and Y. Wang, *Inorg. Chem.*, 2021, **61**, 586–596.
35 P. Chen, X. He, M. Pang, X. Dong, S. Zhao and W. Zhang, *ACS Appl. Mater. Interfaces*, 2020, **12**, 20429–20439.
36 R. J. Marshall, S. L. Griffin, C. Wilson and R. S. Forgan, *Chem.–Eur. J.*, 2016, **22**, 4870–4877.
37 B. Guo, F. Li, C. Wang, L. Zhang and D. Sun, *J. Mater. Chem. A*, 2019, **7**, 13173–13179.
38 Y. Tang, H. Huang, J. Li, W. Xue and C. Zhong, *J. Mater. Chem. A*, 2019, **7**, 18324–18329.
39 X. Zhang, J. Maddock, T. M. Nenoff, M. A. Denecke, S. Yang and M. Schröder, *Chem. Soc. Rev.*, 2022, **51**, 3243–3262.
40 K. Xiong, X. Li, Y. Shi, J. Zhang, Y. Zhang, K. Zhang, M. Wu and Y. Gai, *Inorg. Chem.*, 2021, **60**, 17435–17439.